High Power Laser Science and Engineering, (2024), Vol. 12, e94, 9 pages.
doi:10.1017/hpl.2024.79

HIGH POWER LASER SCIENCE AND ENGINEERING

RESEARCH ARTICLE

Online target normal sheath acceleration proton beam stabilization at 1 Hz in ultra-intense laser–matter interaction

Jose Luis Henares[1], Michael Ehret[1], Jon Apiñaniz[1], Carlos Salgado-López[1], José Antonio Pérez-Hernández[1], María Luisa Berlanga[1], Ana María Cives Fernández[1], Evgeny Filippov[1], Enrique García-García[1], Rubén Hernández Martín[1], Diego De Luis[1], Pilar Puyuelo-Valdes[1], Isabel Rodríguez-Pérez[1], María Dolores Rodríguez Frías[1,2], Iuliana-Mariana Vladisavlevici[1], and Giancarlo Gatti[1]

[1]*CLPU (Centro de Láseres Pulsados), Villamayor, Salamanca, Spain*

[2]*Dpto. Fisica y Matemáticas. Universidad de Alcalá, Madrid, Spain*

(Received 5 July 2024; revised 25 October 2024; accepted 5 November 2024)

Abstract

We introduce a versatile high-repetition-rate solid tape target system suitable for relativistic laser-plasma driven secondary sources. We demonstrate the operation and stability monitoring based on a petawatt laser focused at 1 Hz. Experiments were carried out at the VEGA-3 laser system of the Centro de Láseres Pulsados facility where results for different tape materials and thicknesses are presented. Experimental proton spectra were recorded by a Thomson parabola spectrometer and a time-of-flight detector. In addition, non-invasive detectors, such as a target charging monitor and ionization chamber detectors, were tested as metrology for the stability of the source. Degradation of the proton signal at high-repetition-rate operation was observed and it was solved by online optimization of the relative focus position of the target and laser beam parameters. We report the use of the tape target for bursts of 1000 shots at 1 Hz with mean cut-off energies of about 10 MeV in optimized interaction conditions.

Keywords: high-repetition-rate operation; laser-plasma acceleration; petawatt laser facility; solid target

1. Introduction

The continuous technical and scientific improvement of lasers[1,2] has led to stable short-pulse PW high-repetition-rate (HRR) Ti:sapphire systems[3,4]. If these lasers are tightly focused onto matter, the relativistic interaction yields forward-acceleration of electrons[5], which in turn can trigger pulsed bright ion beams by well-known mechanisms such as target normal sheath acceleration (TNSA)[6,7] and others[8]. The most widely used laser-driven ion acceleration mechanism is TNSA, where an electric field is set due to spatial charge separation (due to the highly energetic electrons leaving the target from the rear side), which drives the acceleration of ions present in the surface contaminants up to several MeV energies[9]. The production of proton and ion beams is beneficial to isotope production[10,11], positron emission tomography[12], ion beam microscopy[13] and particle-induced X-ray emission (PIXE)[14–16], as well as inertial confinement fusion[17], fast ignition schemes[18] and neutron production[19].

Most of these applications require HRR particle production, which poses a challenge for solid-density targets as they have to be replaced after being destroyed by the laser interaction[20]. Several approaches are being pursued, for example, the generation of cryogenic ribbons[21–23], use of liquid jets[24–26], generation of supersonic gas jet targets[27,28] and unwinding of a thin tape near the interaction position[29–42]. All of these schemes provide a fast refresh of the target surface automatically and are able to deliver tens of thousands of targets in continuous operation under high-vacuum conditions. Tape targets stand out for their

Correspondence to: J. L. Henares, CLPU (Centro de Láseres Pulsados), Edificio M5, Parque Científico USAL, C/Adaja, 8, 37185 Villamayor, Salamanca, Spain. Email: jlhenares@clpu.es

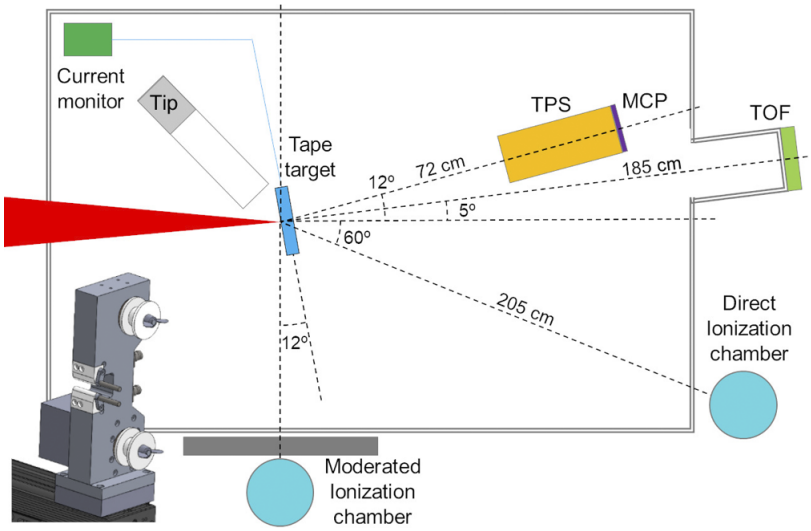

Figure 1. Setup of the tape target experiment and related diagnostics in the VEGA-3 experimental chamber (see text for details). A picture of the tape target system is also shown.

good vacuum compatibility and their flexibility regarding the material. However, common problems arise when tape target systems are used in PW laser facilities. The motors have a high sensitivity to laser-generated electromagnetic pulses (EMPs), which may produce electronic damage and subsequent degradation of the motor performance, and the target suffers from mechanical instability due to the extreme conditions of the interaction. In addition, the large production of debris at an HRR can damage optics and detectors[43]. All of this impedes the use of tape targets at 1 Hz in the focus of PW lasers. Here we present the successful acceleration of multi-MeV proton and ion beams at 1 Hz using an almost 1 PW laser and discuss the stability problems found and ways to solve them[44,45].

2. Experimental setup

The experiment was carried out in the VEGA-3 laser system at the Centro de Láseres Pulsados (CLPU) facility (Spain). The laser system consists of a Ti:sapphire laser ($\lambda = 800$ nm) that can deliver 30 J laser energy, 30 fs temporal duration and up to 1 Hz repetition rate. The laser beam is focused by an $F/11$ off-axis parabolic mirror to a spot of 14 μm full-width at half maximum (FWHM). The energy on the target plane is reduced 21% due to losses in the beam transport after the compressor (giving a total laser power of 0.8 PW on the target plane). This value is extrapolated from calibrations recorded at low energy. In addition, we estimate that 20% of the energy on target is within the FWHM of the first Airy disk, based on images of the focal spot taken at low energy. The laser energy and pulse duration are measured on-shot (the latter using a second harmonic autocorrelator system). The laser energy and pulse duration remained constant throughout this study. The estimated peak intensity used in this study was 1.3×10^{20} W/cm^2. The Strehl ratio measured during the experiment was 0.82 ± 0.01. The laser contrast of VEGA-3 is up to 10^{-12} at 0.1 ns with no significant pre-pulses. The Rayleigh length (Z_R) is 464 ± 145 μm. This parameter will be useful to generalize relative movements along the laser propagation axis. The setup of the experiment is shown in Figure 1.

2.1. High-repetition-rate target

The tape target consists of a motorized wheel that unwinds a thin film. A second wheel recovers the film and maintains the tautness to ensure the target flatness. The target itself is further described in Ref. [45]. Deviations of the target due to the winding movement were measured with a confocal chromatic sensor, ConfocalDT IFS2406-3. These fluctuations were found to be below 25 μm standard deviation in the laser propagation axis, well below the estimated Rayleigh length. The tape target is placed at the laser interaction point with an angle of 12° with respect to the laser forward axis. Two materials have been studied: aluminium and copper (10 and 7.6 μm thickness).

2.2. Particle detectors

A Thomson parabola spectrometer (TPS) coupled to a micro-channel plate (MCP) screen, placed at 12° with respect to the laser forward axis and pointed towards the interaction, was used to characterize the ion emission from the target. A TPS consists of a magnetic dipole followed by a pair of electric plates that allow one to measure the energy distributions of different ion species. The TPS was calibrated by measuring the magnetic field between the plates and then comparing

https://doi.org/10.1017/hpl.2024.79 Published online by Cambridge University Press

with the expected particle trajectories. It was positioned at 72 cm from the tape target with a 200 μm diameter entrance pinhole. More specific information can be found in Ref. [46].

A time-of-flight (TOF) detector is also used to measure the maximum proton energies. It consists of two MCPs with sub-nanosecond rise time. The MCP detector is fitted with a 1.3 in. diameter input grid. The 2.5 in. diameter grid mounting plate presents a flat, field-free plane to the incoming ions. The detector was located at 190 cm from the interaction point in an inclined plane with respect to the equatorial plane at the angles 5° in the horizontal and 9° in the vertical direction. Signals are recorded with a 2 GHz oscilloscope. In addition, non-invasive diagnostics of the beam have been tested in order to seek data for future applications (e.g., irradiation), where neither TPS nor TOF detectors can be used to monitor the particle beam. Two Thermo Scientific ionization chamber (IC) detectors, models FHT190 and FHT192, are installed in the experimental area for radioprotection purposes. These detectors measure the photons generated as secondary radiation from primarily accelerated particles. Both FHT190 and FHT192 are suitable for measurements down to the natural radiation background with noble gas-nitrogen mixture of a volume of 4.25 L and a filling pressure of 7 bars. The system features high-precision ambient equivalent dose measurements in the range between 0.1 μSv/h and 1 Sv/h for photon radiation from 30 keV to 7 MeV energy range. The registered data from the IC is based on a collection of charges created by the direct IC within the gas. It only uses the discrete charges created by each interaction between the incident radiation and the gas. The FHT190 detector was installed close to the experimental chamber at 2.05 m from the interaction point and 60 degrees from the laser propagation axis, while the FHT192 IC was situated approximately at 10 m and 90 degrees from the laser propagation axis. The signal from the latter is moderated with a 58.8 cm standard concrete shielding. For the sake of comparison we will define the first detector (closest to the interaction) as the direct IC detector and the shielded one as the moderated IC detector. Both detectors are useful since the direct IC gives a precise idea of the production of radiation, while the moderated one is better for the optimization method due to its background noise reduction.

The electron ejection as well as the EMP amplitude is diagnosed by a target charging monitor (TCM), which is constructed based on the principles of an inductive current monitor[47,48]. A TCM measures the time derivative of the current between the target and grounding that is guided through the device. Current pulses are excited by laser–plasma interaction, that is, the discharge pulse and pulsed return current EMP in the regime of relativistic laser interaction[49]. For this work, return current EMPs are transported via RG142 coaxial cables and the circuit impedance is $Z = 50\ \Omega$. Cable lengths are measured with ns FWHM voltage pulses: the target and TCM are connected with a coaxial cable of 9.6 ± 0.2 ns length, and the TCM and grounding are connected with a coaxial cable of 13.6 ± 0.1 ns length. Induced signals are transported to a 2 GHz oscilloscope and acquisitions are corrected throughout for the frequency dependent attenuation of circuit elements. Circuit calibrations are done using an R&S ZNH 4 GHz vector network analyser. The effective bandwidth of the circuit is 2 GHz.

3. Results and discussion

The proton signal was analysed by the TPS and TOF detectors for every shot. In the case of the TPS, each ion species shows a parabolic trace and the background was carefully subtracted for each species[50]. From the proton trace, the maximum cut-off energy was calculated. The TOF detector compares the X/gamma-ray signal generated by the laser radiation and the signal generated by the arrival of the particles, obtaining the maximum velocity with the particles closest to the reference and thus the maximum energy. The following studies regard the maximum proton energies measured by the TPS and the TOF detector for several bursts of shots at 1 Hz. Information of the IC and TCM measurements is also indicated in the figures in order to validate their validity and performance.

3.1. Proton signal degradation at an HRR

As can be seen in Figure 2, all diagnostics show the same trend. In detail, the TPS, TOF detector and TCM agree in shot-to-shot details and the IC detectors show a coarse agreement in the general trends. HRR operation (1 Hz) produces an increase and then a degradation of the maximum proton signal measured in all detectors (around the 50th shot in the burst) from a single configuration of parameters with both aluminium and copper targets. The degradation is also clear in both IC detectors and the TCM. An increase of signal in the detectors was observed experimentally when the target was moved along the laser propagation axis (e.g., initial cut-off energies could be recovered in the TPS). We concluded that this degradation comes from a spatial drift of the focal spot when operating at 1 Hz. Thermal nature of this drift is under consideration as the optimal target position comes back to the initial value after some ‘cooling’ time or if the operation is made at single shot. This effect might come from the laser system amplifier or the laser gratings. The same effect was observed whether the amplification pumps were kept running at 1 Hz long before the operation or just during it, indicating that the drift may not be due to thermal lensing in the amplifiers. We are considering thermal effects in the compressor gratings as the most probable origin of the drift. Thermal effects in the laser gratings could also produce spatial chirp and degradation due to spatio-temporal coupling. The thermal effects in the gratings and

https://doi.org/10.1017/hpl.2024.79 Published online by Cambridge University Press

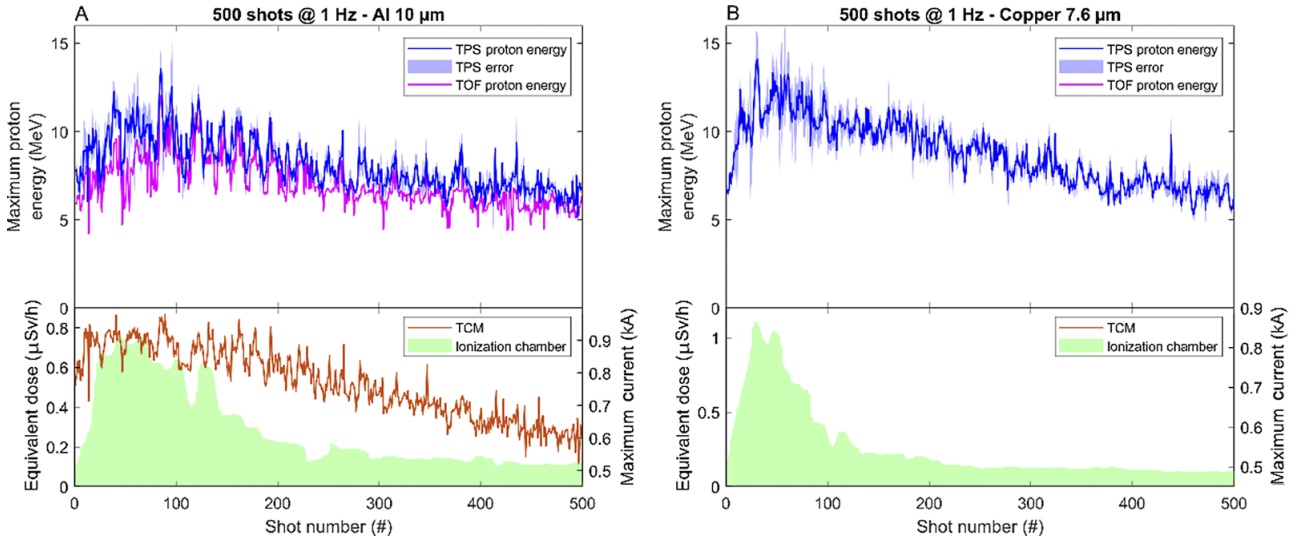

Figure 2. Proton maximum cut-off energy for (a) aluminium and (b) copper targets. Degradation of the signal can be observed in both figures and in all detectors. The maximum proton energy found for the aluminium target is around 11 MeV and decreases up to 6 MeV on average, while for the copper target it is around 13 MeV and decreases up to 7 MeV on average. The direct IC detects for both materials a maximum of about 2×10^4 µSv/h (not shown). In the case of the moderated IC, it measures 0.8 µSv/h (aluminium) and 1.0 µSv/h (copper). The TOF and TCM signals for copper were lost.

the subsequent modifications of the laser beam properties need to be further investigated.

It is also important to remark that aluminium targets produce lower maximum proton energies but a more stable signal in the moderated IC detector, while copper targets generate a higher maximum proton energy but the signal in the moderated IC detector quickly decreases. This is probably because of the thickness difference between both targets.

3.2. *Online optimization*

Two ways were considered to mitigate the thermal effect. One option was to move the target position during operation along the laser axis (longitudinal) to retrieve the real focal spot position. This has the drawback of changing the reference position of the source. The second option was the modification of the collimation lens in the laser system to adapt the divergence of the laser beam. This lens is located between the last amplification stage and the compressor in a motorized stage. This has the drawback of changing the laser wavefront, the diameter of the laser, thus the minimum focal spot achievable, and perhaps adding astigmatism effects. In both cases, it was possible to perform online adaptation in order to retrieve the maximum signal (presumably at the minimum laser spot). Both movements are given in units of Z_R, where the reference zero was defined in the plane of the focal spot at low power and a single shot. Positive increments of Z_R correspond to movements increasing the distance from the off-axis parabolic mirror and vice versa. The effects of movement of the target position and a collimation lens for single shots are shown in Figure 3 using a copper target. In this case, a series of bursts of 10 shots were taken for each parameter. The region of the optimized maximum proton signal for single-shot operation can be clearly distinguished.

It is important to note that motor movement during optimization runs is performed online between shots (thus a 1000-shot run takes 1000 s). Figure 4 shows the relevance of the correction procedure in both cases of signal optimization during an online burst. In Figure 4(a) the target was moved $3Z_R$, $5Z_R$, $8Z_R$ from the original position to retrieve the signal. In the last configuration it is possible to conclude that the spot was still moving as the proton signal slowly increased. Then in Figure 4(b) the collimation lens was used to modify the laser spot position. In this case the target was moved before the run to the $8Z_R$ position with respect to the zero position. It is possible to see that moving from $9Z_R$ to $11Z_R$ decreased the proton signal (meaning the laser spot overtakes the target) and then moving back to $8Z_R$ increased the signal again. Note that the displacement of the focal plane by $8Z_R$ is consistent for both approaches. The magnitude of the displacement mandates a correction not only for ion generation, but also for any HRR experiment. It is important to note that the changes in the proton cut-off energies are well reflected in signals of the moderated IC detector and the TCM, a behaviour correlated with the hot electron temperature, which has already been reported in Ref. [48]. It is also interesting to observe that a change in the target position does not affect differently the signal measured by the TPS and TOF detectors (meaning the divergence of the particle beam remains similar), while modifying the collimation lens also affects the divergence of the beam since there is a change in the properties of the laser propagation (i.e., wavefront quality, focal spot size, etc.). In Figure 4(b) in the range of shots #85–#115, the signal from TPS increases

https://doi.org/10.1017/hpl.2024.79 Published online by Cambridge University Press

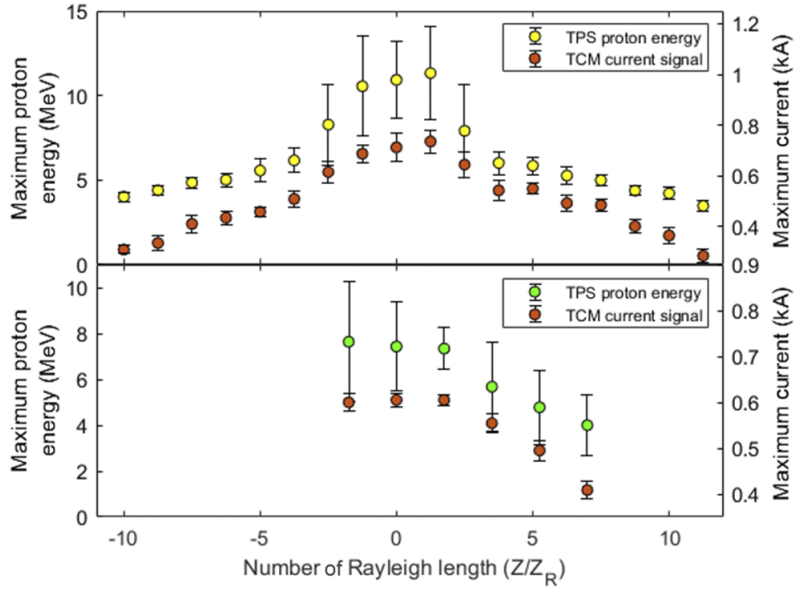

Figure 3. Measurements of the relative displacement from best focus of the Rayleigh length distance Z_R as a function of the maximum proton energies measured in single-shot laser interaction for target position movement (upper figure) and modification of the collimation lens (lower figure). The maximum return current EMP signal measured by the TCM is also shown for the same shots. Each point corresponds to an average of 10 shots with its standard deviation.

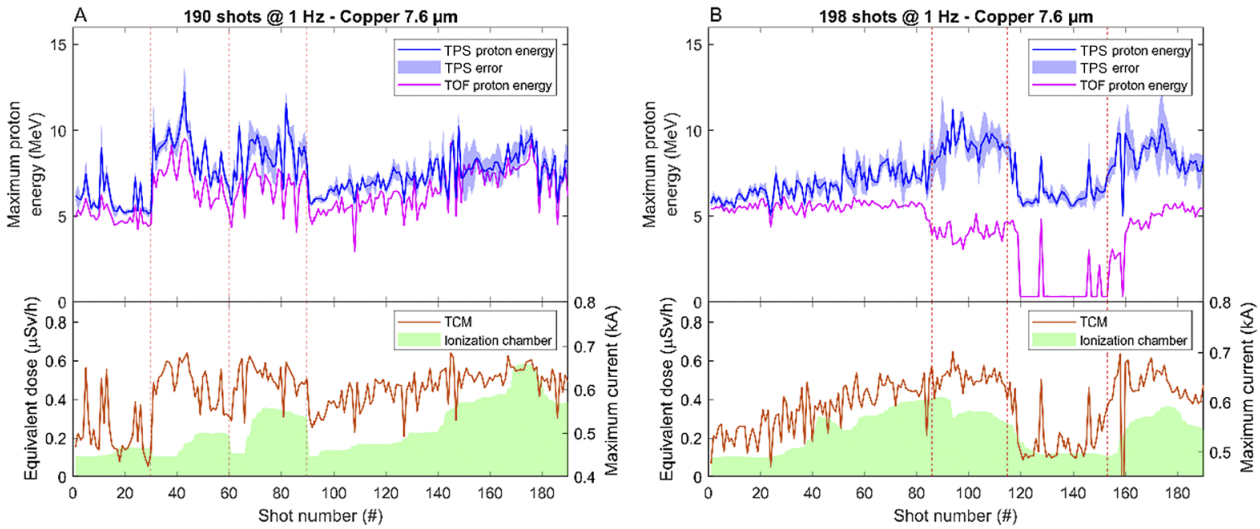

Figure 4. Optimization with (a) target position and (b) laser collimation lens during operation in the copper target. Shot numbers (#) are indicated by red lines. In case (a), the target was moved $3Z_R$ (#30), $5Z_R$ (#60), $8Z_R$ (#90) from the original position to optimize the signal. In (b), the target was moved prior to the run to $8Z_R$ and then the laser focal spot was moved to $9Z_R$ (#86) and then to $11Z_R$ (#115), clearly exceeding the optimum interaction plane. Afterwards the focal spot is moved back to $8Z_R$ (#153).

while decreasing for the TOF detector. This means that more energetic protons are concentrated in the 0 deflection and the divergence of the proton beam is lower. The modification of the collimation lens could be a valuable avenue to control the divergence and collimation of the proton beam, to be studied in future experiments.

3.3. Proton signal stabilization

The *ab initio* adjustment of the target position to the position where the highest laser intensities are expected leads to a stable operation. The predictability of this position is significant, because it allows one to define the corrected position as the source position, for example, for beamlines. In Figures 5(a) and 5(b) the target was moved $9Z_R$ prior to the run to compensate for the gradual defocusing and then small adjustments were done with the collimation lens. It is important to remark that 750 shots at 1 Hz were achieved with the copper target in a stable configuration (Figure 5(b)) of about 9 MeV proton maximum energies. Both the TPS and TOF detector detect the same energies and the TCM can follow the increase and stabilization of the

https://doi.org/10.1017/hpl.2024.79 Published online by Cambridge University Press

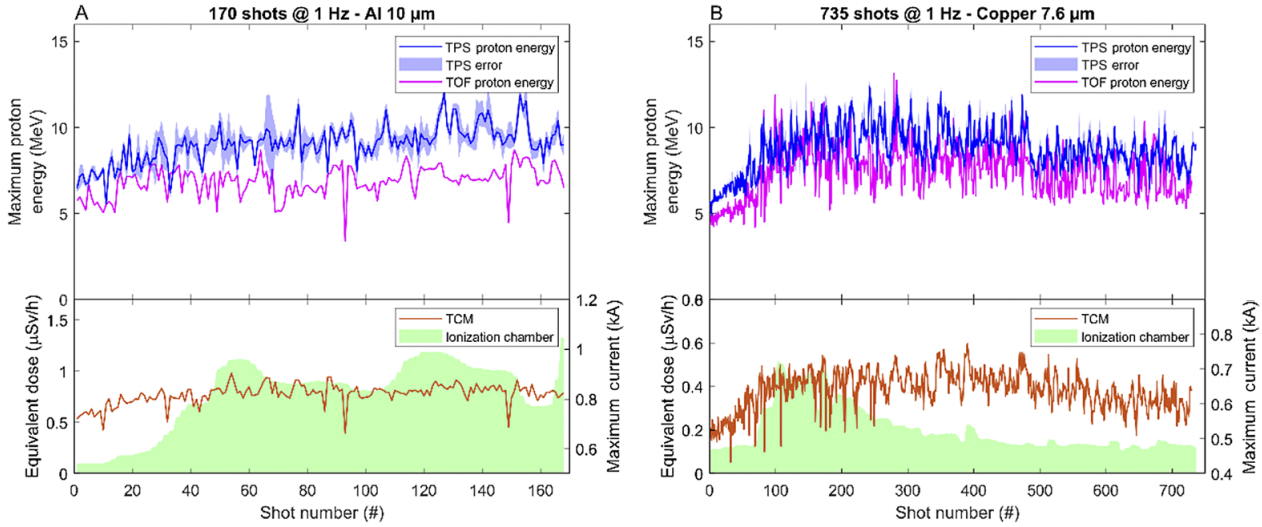

Figure 5. Stabilization of maximum proton signal for aluminium and copper targets. In both cases the target was moved prior to the run to $9Z_R$. The maximum proton energy found for aluminium target is around 10 MeV at the end of the run, while for the copper target it is around 9 MeV. The energy jumps in (b) cannot be explained and both the IC detectors and TCM do not show sharp differences. The direct IC detector measures a maximum of about 2×10^4 µSv/h (aluminium) and 1×10^4 µSv/h (copper) (not shown) and the moderated one 1 µSv/h (aluminium) and 0.5 µSv/h (copper). The maximum return current EMP detected stabilizes around 0.6 kA at the end of the run.

signal. IC detectors show a signal increase, decrease and then stabilization.

In addition, a long run of 1000 shots at 1 Hz was performed to study the reliability of the system (Figure 6). To our knowledge this is the first time that a long run of proton production from metal targets was achieved using a 0.8 PW laser system at 1 Hz. The target was moved prior to the run to $9Z_R$. In order to prove the effect of the collimation lens, it was moved to $5Z_R$ and the signal decreased while it recovered when moving back. In this case, the TPS and TOF detector show a more collimated proton beam since the signal from the TOF detector is smaller on average. This long run proves the stability and reliability of this target for many applications. It is interesting to observe how the TCM perfectly follows the modifications of the parameters and further stabilization. On the same path, the IC detectors measure an increase of signal at the beginning and the stabilization after parameter optimization.

3.4. Diagnostics comparison

A new paradigm in the detection of particles generated by laser–plasma interaction is needed to accomplish effective HRR operation. Here the figure of merit will be used to demonstrate the simultaneous detection of different radiations (and the detection of the same radiations by different means). For this reason, we will compare different diagnostics used during the experiment (TPS, TOF detector, TCM and IC detectors in both direct and moderated modes) in order to quantify their agreement to detect changes in the interaction due to parametric modifications during optimization, and their reliability to measure the stabilization of the source.

In this study, the TPS and TOF detector have a similar detection range from 0.4 to 25 MeV maximum proton energy. In general, the TPS and TOF detector follow similar trends (with the exception of the use of the collimation lens) and a range of values were obtained from 5 up to 16 MeV. In the case of instrumentation for applications, the TPS has the drawback of measuring the direct proton beam, while the TOF detector has the advantage that it can be mounted in an angle sufficiently far away from the propagation axis to use the direct proton beam and still obtain information; however care has to be taken when modifying target or laser parameters.

TCM maximum amplitude measurements range from 0.290 to 1.03 kA. The TCM provided high sensitivity to changes and valuable information about the laser–plasma interaction, and the quality of the expelled electrons (thus proton acceleration). Still more information can be extracted from this detector (e.g., integrated return current signal, oscillations) and it will be further studied.

The IC detectors have a minimum detection threshold of 0.1 µSv/h, which comes from background radiation. The direct IC detector measured up to 38 mSv/h in some punctual cases, while the moderated IC detector measured up to 1.33 µSv/h. The direct IC detector provided peaked distributions with information of the total production of radiation; however, the shot-to-shot oscillations of this signal make it unusable for optimization or evaluation of stabilization. For this reason, it was found that the moderated IC detector was the tool to be used to control changes, stability and reliability of the source. However, it was observed that, due

https://doi.org/10.1017/hpl.2024.79 Published online by Cambridge University Press

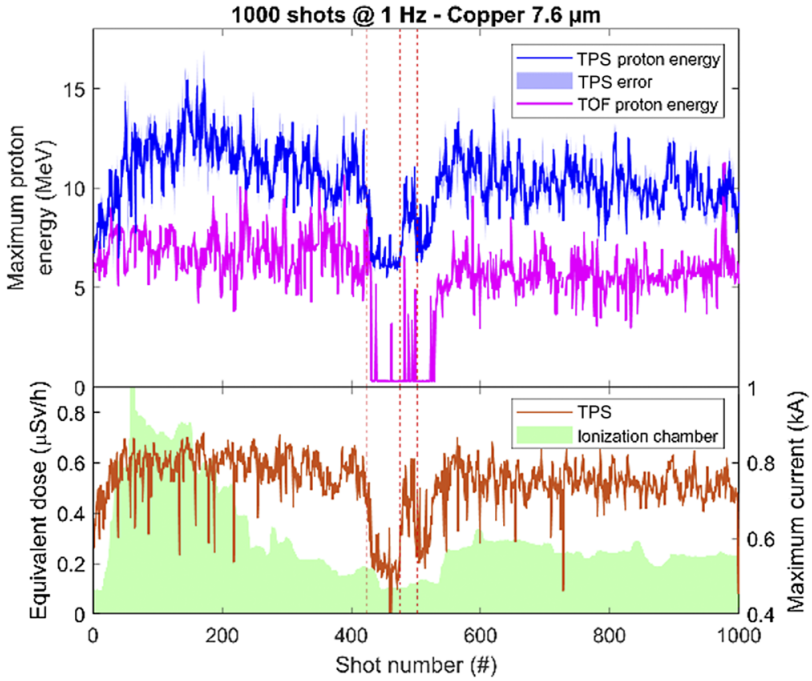

Figure 6. One-thousand shot run of 0.8 PW at 1 Hz. The target was moved prior to the run to $9Z_R$; then the laser focal spot was moved to $5Z_R$ (#423), $7Z_R$ (#475) and back to $9Z_R$ (#502). The signal is stable at 10 MeV (TPS) and 6 MeV (TOF detector). The direct IC detector measures a maximum of about 2.5×10^4 µSv/h (not shown) and the moderated one 0.8 µSv/h. The TCM measures an almost stable 0.75 kA return current EMP.

Table 1. Cases studied with the figure of merit of the last 100 shots to evaluate the stabilization of the source.

Case	Figure 5(a)	Figure 5(b)	Figure 6
Number of shots	170	735	1000
Material	Al	Cu	Cu
TPS proton energy (MeV)	9.4 ± 0.9	8.3 ± 0.8	9.7 ± 0.9
TOF detector proton energy (MeV)	6.9 ± 0.8	6.4 ± 1.2	5.8 ± 1.2
TCM current (kA)	831 ± 32	605 ± 34	735 ± 42
Dir. IC detector dose (mSv/h)	18.13 ± 5.72	0.4 ± 0.2	3.8 ± 1.7
Mod. IC detector dose (µSv/h)	0.91 ± 0.15	0.13 ± 0.01	0.23 ± 0.01

to its nature, the moderated IC detector has some seconds delay with respect to other detectors (clearly observable in Figure 3(a) around shots #30 and #60, and in Figure 4(b) around shot #115). This effect will be further analysed in a following publication.

Three cases will be studied in detail concerning the stabilization of the proton source: 170 shots in Al (Figure 5(a)), 735 shots in Cu (Figure 5(b)) and 1000 shots in Cu (Figure 6). For the sake of comparison all averages will be evaluated by the consecutive last 100 shots for each stabilization case as a figure of merit (Table 1).

All cases in this study obtained similar maximum proton energies (focusing on the stable part) in the TPS and TOF detectors with the exception of the use of the collimation lens parameter (e.g., in Figure 6), which was considered as an effective reduction of the proton beam divergence. It was expected that the IC detectors might be also sensitive to beam divergence effects; however, it is not possible to make a clear conclusion and this will be the topic of future experiments. A similar maximum return current EMP was measured by the TCM in all cases, and this detector proved to be very stable and precise when detecting changes in the interaction efficiency (e.g., in Figure 6 around shot #450). However, there is a behaviour change when both IC detectors were analysed. The direct and moderated IC signals detected are higher in Figure 5(a) compared to lower signals obtained in the other two. This could come from the nature of the target (aluminium) and needs further study with more data. As a conclusion, different diagnostics were compared, observing promising behaviour to measure changes simultaneously. This will be fundamental in order to characterize the performance of a laser–plasma source at HRR.

4. Conclusion

In conclusion, 1 Hz bursts of up to 1000 laser shots produced, for the first time, stable proton beams from metallic foil targets using an almost 1 PW laser, which represents the technological limit of the facility in terms of repetition rate. A degradation of the proton signal has been observed when operating the target at 1 Hz. It was deduced that defocusing of the laser was the origin of the signal degradation and it might come from thermal effects in the laser gratings. The effect of defocusing of the laser was compensated by the use of target motorization and the collimation lens in the laser system. It was found that a modification of the target position does not affect the quality of the beam, while changing the

https://doi.org/10.1017/hpl.2024.79 Published online by Cambridge University Press

collimation lens could modify the divergence of the proton beam. We also consider for future experiments the use of adaptative optics (i.e., deformable mirrors) to mitigate this effect.

In addition, we have identified potential diagnostics to control and optimize the particle source online, allowing its use for applications. The TCM and IC detectors have proven their reliability and stability working in this harsh environment and to measure changes in the laser–plasma interaction conditions at 1 Hz. At this point other problems can arise, such as degradation of the optics and detectors in the experimental chamber due to the large production of debris and particles. We can conclude that the working principle of HRR targets at 1 Hz for laser–plasma proton production has been demonstrated.

Author contributions

JLH, ME, CS, IMV, PP, AMC, JAP-H and EG performed the data acquisition and curation; JLH and ME wrote the first draft of the manuscript; JLH organized the beamtime at CLPU; JLH, ME, RH and DL managed implementation of the device; JLH, ME, JIA, CS, RH, DL and PP contributed to the conception and design of the study; JLH, ME, JIA, MLB, AMC, EF, IR and IMV performed the analysis; all authors were involved with underlying experimental work; all authors contributed to manuscript improvement, read and approved the submitted version.

Acknowledgements

This work would not have been possible without the help of the laser and the engineering teams at CLPU. This work received funding from the European Union's Horizon 2020 research and innovation programme through the European IMPULSE project under grant agreement No. 871161 and from LASERLAB-EUROPE V under grant agreement No. 871124. It benefited from funding from the Ministerio de Ciencia, Innovación y Universidades in Spain, through ICTS Equipment grant No. EQC2018-005230-P, further from grant PID2021-125389OA-I00 funded by MCIN / AEI / 10.13039/501100011033 / FEDER, UE, and by 'ERDF A way of making Europe', by the European Union and in addition from grants from the Junta de Castilla y León, No. CLP263P20 and No. CLP087U16. This paper is based upon work from COST (European Cooperation in Science and Technology) Action CA21128-PROBONO 'PROton BOron Nuclear fusion: from energy production to medical applicatiOns', supported by COST.

References

1. T. H. Maiman, Nature **187**, 493 (1966).
2. M. DiDomenico, J. E. Geusic, H. M. Marcos, and R. G. Smith, Appl. Phys. Lett. **8**, 180 (1966).
3. P. Maine, D. Strickland, P. Bado, M. Pessot, and G. Mourou, IEEE J. Quantum Electron. **24**, 398 (1988).
4. M. Aoyama, K. Yamakawa, Y. Akahane, J. Ma, N. Inoue, H. Ueda, and H. Kiriyama, Opt. Lett. **28**, 1594 (2003).
5. T. Tajima and V. Malka, Plasma Phys. Control. Fusion **62**, 034004 (2012).
6. R. A. Snavely, M. H. Key, S. P. Hatchett, T. E. Cowan, M. Roth, T. W. Phillips, M. A. Stoyer, E. A. Henry, T. C. Sangster, M. S. Singh, S. C. Wilks, A. MacKinnon, A. Offenberger, D. M. Pennington, K. Yasuike, A. B. Langdon, B. F. Lasinski, J. Johnson, M. D. Perry, and E. M. Campbell, Phys. Rev. Lett. **85**, 2945 (2000).
7. S. C. Wilks, A. B. Langdon, T. E. Cowan, M. Roth, M. Singh, S. Hatchett, M. H. Key, D. Pennington, A. MacKinnon, and R. A. Snavely, Phys. Plasmas **8**, 542 (2001).
8. T. Esirkepov, M. Borghesi, S. V. Bulanov, G. Mourou, and T. Tajima, Phys. Rev. Lett. **92**, 175003 (2004).
9. M. Borghesi, Springer Proc. Phys. **231**, 143 (2019).
10. K. Nemoto, A. Maksimchuk, S. Banerjee, K. Flippo, G. Mourou, D. Umstadter, and V. Yu. Bychenkov, Appl. Phys. Lett. **78**, 595 (2001).
11. Z. Sun, AIP Adv. **11**, 040701 (2021).
12. M. I. K. Santala, M. Zepf, F. N. Beg, E. L. Clark, A. E. Dangor, K. Krushelnick, M. Tatarakis, I. Watts, K. W. D. Ledingham, T. McCanny, I. Spencer, A. C. Machacek, R. Allott, R. J. Clarke, and P. A. Norreys, Appl. Phys. Lett. **78**, 19 (2001).
13. F. E. Merrill, A. A. Golubev, F. G. Mariam, V. I. Turtikov, and D. Varentsov, AIP Conf. Proc. **1195**, 667 (2009).
14. F. Mirani, A. Maffini, F. Casamichiela, A. Pazzaglia, A. Formenti, D. Dellasega, V. Russo, D. Vavassori, D. Bortot, M. Huault, G. Zeraouli, V. Ospina, S. Malko, J. I. Apiñaniz, J. A. Pérez-Hernández, D. De Luis, G. Gatti, L. Volpe, A. Pola, and M. Passoni, Sci. Adv. **7**, eabc8660 (2021).
15. M. Barberio and P. Antici, Sci. Rep. **9**, 2045 (2019).
16. M. Salvadori, F. Brandi, L. Labate, F. Baffigi, L. Fulgentini, P. Galizia, P. Koester, D. Palla, D. Sciti, and L. A. Gizzi, Phys. Rev. Appl. **21**, 064020 (2024).
17. M. Roth, T. E. Cowan, M. H. Key, S. P. Hatchett, C. Brown, W. Fountain, J. Johnson, D. M. Pennington, R. A. Snavely, S. C. Wilks, K. Yasuike, H. Ruhl, F. Pegoraro, S. V. Bulanov, E. M. Campbell, M. D. Perry, and H. Powell, Phys. Rev. Lett. **86**, 436 (2001).
18. M. Tabak, D. S. Clark, S. P. Hatchett, M. H. Key, B. F. Lasinski, R. A. Snavely, S. C. Wilks, R. P. J. Town, R. Stephens, E. M. Campbell, R. Kodama, K. Mima, K. A. Tanaka, S. Atzeni, and R. Freeman, Phys. Plasmas **12**, 057305 (2005).
19. F. Negoita, M. Roth, P. G. Thirolf, S. Tudisco, F. Hannachi, S. Moustaizis, I. Pomerantz, P. Mckenna, J. Fuchs, K. Sphor, G. Acbas, A. Anzalone, P. Audebert, S. Balascuta, F. Cappuzzello, M. O. Cernaianu, S. Chen, I. Dancus, R. Freeman, H. Geissel, P. Ghenuche, L. Gizzi, F. Gobet, G. Gosselin, M. Gugiu, D. Higginson, E. D'Humières, C. Ivan, D. Jaroszynski, S. Kar, L. Lamia, V. Leca, L. Neagu, G. Lanzalone, V. Meot, S. R. Mirfayzi, I. O. Mitu, P. Morel, C. Murphy, C. Petcu, H. Petrascu, C. Petrone, P. Raczka, M. Risca, F. Rotaru, J. J. Santos, D. Schumacher, D. Stutman, M. Tarisien, M. Tataru, B. Tatulea, I. C. E. Turcu, M. Versteegen, D. Ursescu, S. Gales, and N. V. Zamfir, arXiv:2201.01068 (2022).
20. M. Ehret, J. I. Apiñaniz, J. L. Henares, R. Lera, D. de Luis, J. A. Pérez-Hernández, L. Volpe, and G. Gatti, Nucl. Instrum. Methods Phys. Res. Sect. B **541**, 165 (2023).
21. S. Garcia, D. Chatain, and J. P. Perin, Laser Part. Beams **32**, 569 (2014).
22. D. Margarone, A. Velyhan, J. Dostal, J. Ullschmied, J. P. Perin, D. Chatain, S. Garcia, P. Bonnay, T. Pisarczyk, R. Dudzak, M. Rosinski, J. Krasa, L. Giuffrida, J. Prokupek, V. Scuderi, J. Psikal, M. Kucharik, M. De Marco, J. Cikhardt, E. Krousky, Z.

https://doi.org/10.1017/hpl.2024.79 Published online by Cambridge University Press

Kalinowska, T. Chodukowski, G. A. P. Cirrone, and G. Korn, Phys. Rev. X **6**, 041030 (2016).
23. M. Rehwald, S. Assenbaum, C. Bernert, F. E. Brack, M. Bussmann, T. E. Cowan, C. B. Curry, F. Fiuza, M. Garten, L. Gaus, M. Gauthier, S. Göde, I. Göthel, S. H. Glenzer, L. Huang, A. Huebl, J. B. Kim, T. Kluge, S. Kraft, F. Kroll, J. Metzkes-Ng, T. Miethlinger, M. Loeser, L. Obst-Huebl, M. Reimold, H. P. Schlenvoigt, C. Schoenwaelder, U. Schramm, M. Siebold, F. Treffert, L. Yang, T. Ziegler, and K. Zeil, Nat. Commun. **14**, 4009 (2023).
24. P. Hilz, T. M. Ostermayr, A. Huebl, V. Bagnoud, B. Borm, M. Bussmann, M. Gallei, J. Gebhard, D. Haffa, J. Hartmann, T. Kluge, F. H. Lindner, P. Neumayr, C. G. Schaefer, U. Schramm, P. G. Thirolf, T. F. Rösch, F. Wagner, B. Zielbauer, and J. Schreiber, Nat. Commun. **9**, 423 (2018).
25. J. T. Morrison, S. Feister, K. D. Frische, D. R. Austin, G. K. Ngirmang, N. R. Murphy, C. Orban, E. A. Chowdhury, and W. M. Roquemore, New J. Phys. **20**, 022001 (2018).
26. P. Puyuelo-Valdes, D. de Luis, J. Hernandez, J. I. Apiñaniz, A. Curcio, J. L. Henares, M. Huault, J. A. Pérez-Hernández, L. Roso, and G. Gatti, Plasma Phys. Control. Fusion **64**, 054003 (2022).
27. J. L. Henares, P. Puyuelo-Valdes, C. Salgado-López, J. I. Apiñaniz, P. Bradford, F. Consoli, D. de Luis, M. Ehret, F. Hannachi, R. Hernández-Martín, A. Huber, L. Lancia, M. Mackeviciute, A. Maitrallain, J.-R. Marquès, J. A. Pérez-Hernández, C. Santos, J. J. Santos, V. Stankevic, M. Tarisien, V. Tomkus, L. Volpe, and G. Gatti, J. Plasma Phys. **89**, 965890601 (2023).
28. V. Ospina-Bohórquez, C. Salgado-López, M. Ehret, S. Malko, M. Salvadori, T. Pisarczyk, T. Chodukowski, Z. Rusiniak, M. Krupka, P. Guillon, M. Lendrin, G. Pérez-Callejo, C. Vlachos, F. Hannachi, M. Tarisien, F. Consoli, C. Verona, G. Prestopino, J. Dostal, R. Dudzak, J. L. Henares, J. I. Apiñaniz, D. De Luis, A. Debayle, J. Caron, T. Ceccotti, R. Hernández-Martín, J. Hernández-Toro, M. Huault, A. Martín-López, C. Méndez, T.-H. Nguyen-Bui, J. A. Perez-Hernández, X. Vaisseau, O. Varela, L. Volpe, L. Gremillet, and J. J. Santos, Phys. Rev. Research **6**, 023268 (2024).
29. S. J. Haney, K. W. Berger, G. D. Kubiak, P. D. Rockett, and J. Hunter, Appl. Opt. **32**, 6934 (1993).
30. P. McKenna, K. W. D. Ledingham, I. Spencer, T. McCany, R. P. Singhal, C. Ziener, P. S. Foster, E. J. Divall, C. J. Hooker, D. Neely, A. J. Langley, R. J. Clarke, P. A. Norreys, K. Krushelnick, and E. L. Clark, Rev. Sci. Instrum. **73**, 4176 (2002).
31. T. Nayuki, Y. Oishi, T. Fujii, K. Nemoto, T. Kayoiji, Y. Okano, Y. Hironaka, K. G. Nakamura, K. Kondo, and K. Ueda, Rev. Sci. Instrum. **74**, 3293 (2003).
32. M. Noaman-ul-Haq, H. Ahmed, T. Sokollik, L. Yu, Z. Liu, X. Yuan, F. Yuan, M. Mirzaie, X. Ge, L. Chen, and J. Zhang, Phys. Rev. Accel. Beams **20**, 041301 (2017).
33. Y. Gao, J. Bin, D. Haffa, C. Kreuzer, J. Hartmann, M. Speicher, F. H. Lindner, T. M. Ostermayr, P. Hilz, T. F. Rösch, S. Lehrack, F. Englbrecht, S. Seuferling, M. Gilljohann, H. Ding, W. Ma, K. Parodi, and J. Schreiber, High Power Laser Sci. Eng. **5**, e12 (2017).
34. S. Raschke, S. Spickermann, T. Toncian, M. Swantusch, J. Boeker, U. Giesen, G. Iliakis, O. Willi, and F. Boege, Sci. Rep. **6**, 32441 (2016).
35. J. Ehlert, M. Piel, F. Boege, M. Cerchez, R. Haas, G. E. Iliakis, R. Prasad, O. Willi, and C. Monzel, AIP Adv. **11**, 065208 (2021).
36. N. P. Dover, M. Nishiuchi, H. Sakaki, Ko. Kondo, H. F. Lowe, M. A. Alkhimova, E. J. Ditter, O. C. Ettlinger, A. Ya. Faenov, M. Hata, G. S. Hicks, N. Iwata, H. Kiriyama, J. K. Koga, T. Miyahara, Z. Najmudin, T. A. Pikuz, A. S. Pirozhkov, A. Sagisaka, U. Schramm, Y. Sentoku, Y. Watanabe, T. Ziegler, K. Zeil, M. Kando, and K. Kondo, High Energy Density Phys. **37**, 100847 (2020).
37. S. Steinke, J. H. Bin, J. Park, Q. Ji, K. Nakamura, A. J. Gonsalves, S. S. Bulanov, M. Thévenet, C. Toth, J.-L. Vay, C. B. Schroeder, C. G. R. Geddes, E. Esarey, T. Schenkel, and W. P. Leemans, Phys. Rev. Accel. Beams **23**, 021302 (2020).
38. F. P. Condamine, N. Jourdain, J. C. Hernandez, M. Taylor, H. Bohlin, A. Fajstavr, T. M. Jeong, D. Kumar, T. Laštovička, O. Renner, and S. Weber, Rev. Sci. Instrum. **90**, 063504 (2021).
39. N. Xu, M. J. V. Streeter, O. C. Ettlinger, H. Ahmed, S. Astbury, M. Borghesi, N. Bourgeois, C. B. Curry, S. J. D. Dann, N. P. Dover, T. Dzelzainis, V. Istokskaia, M. Gauthier, L. Giuffrida, G. D. Glenn, S. H. Glenzer, R. J. Gray, J. S. Green, G. S. Hicks, C. Hyland, M. King, B. Loughran, D. Margarone, O. McCusker, P. McKenna, C. Parisuaña, P. Parsons, C. Spindloe, D. R. Symes, F. Treffert, C. A. J. Palmer, and Z. Najmudin, High Power Laser Sci. Eng. **11**, e23 (2023).
40. J. Peñas, A. Bembibre, D. Cortina-Gil, L. Martín, A. Reija, C. Ruiz, M. Seimetz, A. Alejo, and J. Benlliure, High Power Laser Sci. Eng. **12**, e22 (2024).
41. J. Peñas, A. Alejo, A. Bembibre, J. I. Apiñaniz, E. García-García, C. Guerrero, J. L. Henares, I. Hernández-Palmero, C. Méndez, M. Á. Millán-Callado, P. Puyuelo-Valdés, M. Seimetz, and J. Benlliure, Sci. Rep. **14**, 11448 (2024).
42. G. Zeraouli, D. A. Mariscal, R. Hollinger, S. Zahedpour Anaraki, E. N. Folsom, E. Grace, D. Rusby, M. P. Hill, G. J. Williams, G. G. Scott, B. Sullivan, S. Wang, J. King, K. K. Swanson, R. A. Simpson, B. Z. Djordjevic, S. Andrews, R. Costa, B. Cauble, F. Albert, J. J. Rocca, and T. Ma, Rev. Sci. Instrum. **94**, 123306 (2023).
43. I. M. Vladisavlevici, C. Vlachos, J. L. Dubois, A. Huerta, S. Agarwal, H. Ahmed, J. I. Apiñaniz, M. Cernaianu, M. Gugiu, M. Krupka, R. Lera, A. Morabito, D. Sangwan, D. Ursescu, A. Curcio, N. Fefeu, J. A. Pérez-Hernández, T. Vacek, P. Vicente, N. Woolsey, G. Gatti, M. D. Rodríguez-Frías, J. J. Santos, P. W. Bradford, and M. Ehret, arXiv:2403.10431 (2024).
44. E. A. Vishnyakov, A. Sagisaka, K. Ogura, T. Zh. Esirkepov, B. Gonzalez-Izquierdo, C. D. Armstrong, T. A. Pikuz, S. A. Pikuz, W. Yan, T. M. Jeong, S. Singh, P. Hadjisolomou, O. Finke, G. M. Grittani, M. Nevrkla, C. M. Lazzarini, A. Velyhan, T. Hayakawa, Y. Fukuda, J. K. Koga, M. Ishino, K. Kondo, Y. Miyasaka, A. Kon, M. Nishikino, Y. V. Nosach, D. Khikhlukha, I. P. Tsygvintsev, D. Kumar, J. Nejdl, D. Margarone, P. V. Sasorov, S. Weber, M. Kando, H. Kiriyama, Y. Kato, G. Korn, K. Kondo, S. V. Bulanov, T. Kawachi, and A. S. Pirozhkov, High Power Laser Sci. Eng., **12**, e32 (2024).
45. M. Ehret, D. De Luis, J. I. Apiñaniz, J. L. Henares, R. Lera, J. A. Pérez-Hernández, P. Puyuelo-Valdes, L. Volpe, and G. Gatti, Plasma Phys. Control. Fusion **66**, 045003 (2024).
46. C. Salgado-López, J. I. Apiñaniz, J. L Henares, J. A. Pérez-Hernández, D. De Luis, L. Volpe, and G. Gatti, Sensors **22**, 3239 (2022).
47. J. Cikhardt, J. Krása, M. De Marco, M. Pfeifer, A. Velyhan, E. Krouský, B. Cikhardtová, D. Řezáč, J. Ullschmied, J. Skála, P. Kubeš, and J. Kravárik, Rev. Sci. Instrum. **85**, 103507 (2014).
48. M. Ehret, J. Cikhardt, P. W. Bradford, I. M. Vladisavlevici, T. Burian, D. De Luis, J. L. Henares, R. Hernández Martín, J. I. Apiñaniz, R. Lera, J. A. Pérez-Hernández, J. J. Santos, and G. Gatti, High Power Laser Sci. Eng. **12**, e33 (2024).
49. M. Ehret, M. Bailly-Grandvaux, P. Korneev, J. I. Apiñaniz, C. Brabetz, A. Morace, P. Bradford, E. d'Humières, G. Schaumann, V. Bagnoud, S. Malko, K. Matveevskii, M. Roth, L. Volpe, N. C. Woolsey, and J. J. Santos, Phys. Plasmas **30**, 013105 (2023).
50. P. Puyuelo-Valdes, J. L. Henares, F. Hannachi, T. Ceccotti, J. Domange, M. Ehret, E. d'Humieres, L. Lancia, J.-R. Marquès, X. Ribeyre, J. J. Santos, V. Tikhonchuk, and M. Tarisien, Phys. Plasmas **26**, 123109 (2019).

https://doi.org/10.1017/hpl.2024.79 Published online by Cambridge University Press